STABILITY, CLEFTING AND OTHER ISSUES RELATED TO UNDESIRED EQUILIBRIA IN LARGE PUMPKIN BALLOONS

Frank Baginski*
George Washington University
Washington, DC 20052
baginski@gwu.edu

Kenneth A. Brakke
Mathematics Department
Susquehanna University
Selinsgrove, PA 17870

Willi W. Schur†
P.O. Box 698
Accomac, VA 23301

29 June 2004

Abstract

NASA's effort to develop a large payload, high altitude, long duration balloon, the Ultra Long Duration Balloon, focuses on a pumpkin shape super-pressure design. It has been observed that a pumpkin balloon may be unable to pressurize into the desired cyclically symmetric equilibrium configuration, settling into a distorted, undesired state instead. Hoop stress considerations in the pumpkin design leads to choosing the lowest possible bulge radius, while robust deployment is favored by a large bulge radius. Some qualitative understanding of design aspects on undesired equilibria in pumpkin balloons has been obtained via small-scale balloon testing. Poorly deploying balloons have clefts, but most gores away from the cleft deploy uniformly. Mechanical locking may be a contributing factor in the formation of such undesired equilibria. Long term success of the pumpkin balloon for NASA requires a thorough understanding of the phenomenon of multiple stable equilibria. This paper uses the notion of stability to classify balloon designs. When we applied our model to a balloon based on the NASA Phase IV-A pumpkin design, we found the fully inflated/fully deployed strained equilibrium float configuration to be unstable. To explore the sensitivity of this particular design and to demonstrate our general approach, we carry out a number of parametric studies that are variations on the Phase IV-A design. In this paper, we will focus on analytical studies, but we also compare our results with experimental and flight data whenever possible. We will discuss the connection between stability and the generic deployment problem.

*Senior Member AIAA

†Member AIAA

1 Introduction

The pumpkin shape balloon concept for a super-pressure balloon seeks structural efficiency in a heterogeneous balloon structure by assigning the global pressure confining strength primarily to a system of load tendons with the load-carrying role of the skin being primarily the transfer of the pressure load to the tendons. Within this rather broad description of the pumpkin shape balloon, designs can differ in a number ways, depending on: (1) the nature and the relative stiffness of the structural materials (both skin and tendons), (2) on considerations given to fabrication, (3) on measures taken to ensure proper deployment and pressurization at altitude and the maintenance of that proper equilibrium configuration throughout service-life pressure-cycling. For clarity of exposition, we use the pumpkin gore shape generation process as presented in [1] to generate families of balloon design shapes that we analyze. The model in [1] includes an improvement over the standard natural-shape assumption of zero hoop stress by taking into account hoop-wise forces that are generated by skin stress resultants and the local half-bulge angle. For practical reasons, gores are made of flat sheets, but it is conceivable to use molded gores if fabrication difficulties and fabrication costs are of no consideration. The equivalent of a molded gore could be achieved by fabricating such a super-gore from several flat sheets that, when seamed together and inflated, approximates the desired shape. See [2] for more on the molded super-gore construction. A doubly-curved representation of a pumpkin gore is shown in Figure 1. The "spine" (centerline) of the deformed pumpkin gore is isometric to the centerline of the lay-flat pattern. A "rib" in the deformed pumpkin gore is isometric to the corresponding segment that is transverse to the centerline in

Figure 1: Pumpkin gore with lay-flat configuration.

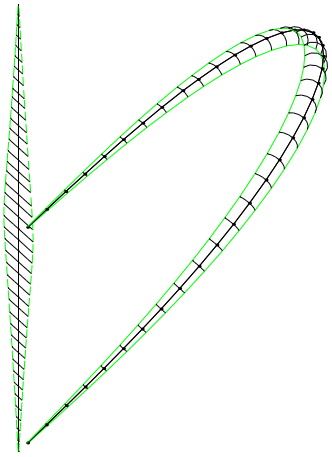

the lay-flat pattern. Hence, the edge of the lay-flat gore is significantly longer than the edge of the doubly-curved deformed pumpkin gore. By fore-shortening the tendons, the proper pumpkin gore geometry can be achieved once the balloon is deployed and fully inflated (see [3]).

At full inflation and pressurization of the pumpkin balloon, there is only one desired equilibrium state, and that is a cyclically symmetric state where all gores are fully deployed. This state is, however, not guaranteed for an arbitrary design of a pumpkin shape balloon. In fact, by design, the pumpkin shape balloon has excess balloon skin relative to minimum volume enclosure, which may provide an opportunity for the existence of multiple equilibria at full inflation and pressurization. The undesired equilibria can be of two types. Either type must be avoided by the design throughout the service life of the balloon. Only the cyclically symmetric configuration is acceptable at full pressurization.

The first type of undesired equilibria appears to be inflation path independent or nearly so. In that case, configurations exist in the vicinity of the desired equilibrium that have equal or lower total potential energy than the desired equilibrium. Vulnerability of a design to this threat can be investigated by a stability analyses of the desired equilibrium configuration. In a long-duration balloon flight, this can occur even if the balloon deployed initially into a cyclically symmetric configuration. Subsequent straining alters the configuration so that the cyclically symmetric configuration is no more a minimum energy state. In that case, migration from the cyclically symmetric equilibrium occurs spontaneously, possibly rapidly.

The second type of undesired equilibria is clearly inflation path dependent. It occurs during ascent when three or more layers of film get mechanically locked and the locking is robust, preventing dislodging of the locked gores by the hoop-wise tension forces that are generated by the flattened gores. In this case, a robustly stable equilibrium is reached that, in configuration space, is far removed from the desired equilibrium state. To picture this flawed configuration, one can envision a Z-fold of 3K gores (K an integer). K gores are folded back behind the outer layer of K gores, then K more gores are folded behind the second layer. By locking under the internal pressure, this K gore wide Z-fold resists the horizontal forces that are generated by the hoop-wise tension in the film. Earlier work (see [4]) indicated that in a pumpkin balloon with several gores swallowed up, the hoop-wise restoring forces are relatively small, especially when compared with the response in a similarly sized zero-pressure natural shape balloon.

It appears that for a given class of balloon designs, both threats to proper deployment and pressurization increase with the number of gores in the balloon and both the distribution and amplitude of gore-width excess relative to minimum volume enclosure. These observations will be affirmed with numerical simulations in this paper.

To avoid the first threat, a design must be such that the cyclically symmetric configuration at full inflation and pressurization is stable. We say that an equilibrium shape $\mathcal{S}$ is stable if all the eigenvalues of the Hessian of the balloon potential energy are positive (see Section 3). If the film is linearly elastic then analysis of this threat can be limited to the stability analysis of the fully inflated/fully deployed strained equilibrium configuration.

Existing data on 48 gore test balloons has shown that a 48 gore constant bulge radius balloon with a bulge angle at the equator near 180 degrees will fully deploy into a robustly stable cyclically symmetric equilibrium even for a test vehicle that has fabrication imperfections, while a constant bulge angle design at a rather modest bulge angle was clearly on the threshold between proper and improper deployment. The sensitivity to both amplitude of excess gore-width and its distribution along the gore length has been further demonstrated on other test vehicles. To quantify this sensitivity, we considered a number of parametric studies where the width of the nominal lay-flat pattern was altered, and the stability of the corresponding fully inflated shape was determined. See [5] for a further discussion on experiments involving small test vehicles or [4] for more on deployment related issues.

In this paper, we will focus on fully inflated shapes arising from a class of pumpkin designs that are related to the NASA Phase IV-A ULDB. Flight 517NT, a Phase IV-A 0.6 million cubic meter pumpkin balloon launched in March 2003 experienced a deployment problem. A cleft that was present in the launch configuration persisted throughout the ascent phase and was maintained once the balloon reached float altitude (see, Figure 2). The sec-

Figure 2: Cleft in Flight 517. Photograph provided by the NASA Balloon Program Office.

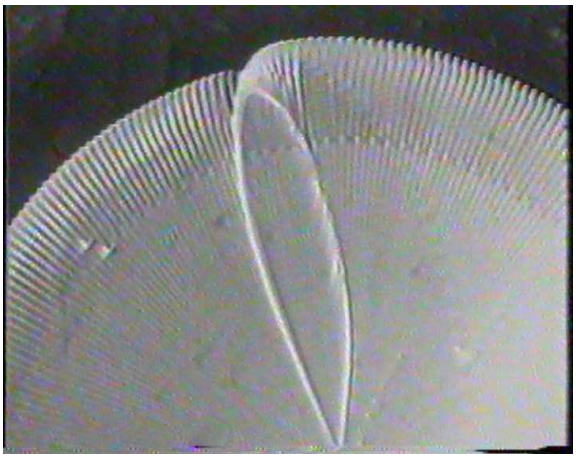

ond Phase IV balloon (Flight 496NT in March 2001) also had deployment problems, assuming an anomalous configuration at maximum altitude. In our concluding remarks, we discuss the connection between stability and undesired equilibria. The reason for first focusing on the fully deployed configuration is clear. If a balloon design leads to an unstable equilibrium configuration at float, then one is inviting trouble. If the balloon design leads to an unstable cyclically symmetric equilibrium configuration at full inflation and under pressurization any time during its service life, then at such instant the configuration will likely depart into an undesired shape with stress resultants far larger than anticipated by the design. The balloon is doomed. The existence of an equilibrium with a lower total potential energy than the cyclically symmetric equilibrium is similarly troublesome, even if the cyclically symmetric equilibrium is at a local minimum of the total potential energy. Through numerical studies, we hope to gain some insight into those factors that promote proper deployment as well as those factors that inhibit proper deployment.

We implemented a model for a strained pumpkin balloon into *Surface Evolver*, an interactive software package [6] for the study of curves and surfaces shaped by energy minimization. If $\mathcal{E}$ is the total potential energy of a balloon configuration $\mathcal{S}$, and $H_{\mathcal{E}}(\mathcal{S})$ is the the Hessian of $\mathcal{E}$ evaluated at $\mathcal{S}$, the eigenvalues of $H_{\mathcal{E}}(\mathcal{S})$ determine the stability of $\mathcal{S}$ (see Section 3). In [7], we explored stability as a function of the design parameters (n_g, r_B) and the uniform tendon slackness parameter ε_t. However, other parameters are equally important. In a long duration flight, the balloon will experience many diurnal cycles, where the constant pressure term will vary from a maximum value during the day to a minimum value at night. In the present paper, we further explore the stability of equilibrium configurations as a function of these and other parameters. We use the stability plot associated with the (n_g, r_B)-parameter space and nominal parameter values as a baseline defining stable and unstable regions. Sensitivity to parameter change is best illustrated by how the interface between the stable and unstable region changes from the nominal state.

2 Finite element model

In this section, we formulate the problem of determining the equilibrium shape of a strained balloon. We have applied this model to pumpkin balloons and we refer the reader to [8] for a more detailed exposition. We will assume that a balloon is situated in such a way that the center of the nadir fitting is located at the origin of a Cartesian coordinate system. If a balloon has n_g gores, then we assume that $y = 0$ is a plane of reflectional symmetry and we model $n_g/2$ gores. The boundary conditions are $y = 0$ for nodes that lie on the boundary of one-half the balloon. The nadir fitting is fixed, and the apex fitting is free to slide up and down the z-axis. The nadir and apex fittings are assumed to be rigid. The total potential energy $\mathcal{E}$ of a strained inflated balloon configuration $\mathcal{S}$ is the sum of six terms,

$$\mathcal{E}(\mathcal{S}) = \mathcal{E}_P + \mathcal{E}_f + \mathcal{E}_t + \mathcal{E}_{top} + S_t^* + S_f^* \tag{1}$$

where

$$\mathcal{E}_P(\mathcal{S}) = -\int_{\mathcal{S}} (\tfrac{1}{2} b z^2 + P_0 z)\mathbf{k} \cdot d\vec{S}, \tag{2}$$

$$\mathcal{E}_f(\mathcal{S}) = \int_{\mathcal{S}} w_f z dA, \tag{3}$$

$$\mathcal{E}_t(\mathcal{S}) = \int_{\Gamma \in \mathcal{S}} w_t \tau(s) \cdot \mathbf{k} \; ds, \tag{4}$$

$$\mathcal{E}_{top} = w_{top} z_{top}, \tag{5}$$

$$S_f^*(\mathcal{S}) = \int_{\mathcal{S}} W_f^* \, dA, \tag{6}$$

$$S_t^*(\mathcal{S}) = \int_{\Gamma \in \mathcal{S}} W_t^* \, ds, \tag{7}$$

$\mathcal{E}_P$ is the hydrostatic pressure potential due to the lifting gas, $\mathcal{E}_f$ is the gravitational potential energy of the film, $\mathcal{E}_t$ is the gravitational potential energy of the load tendons, $\mathcal{E}_{top}$ is the gravitational potential energy of the apex fitting, S_t^* is the relaxed strain energy of the tendons, and S_f^* is the relaxed strain energy of the balloon film, P_0 is the differential pressure at the base of the balloon where $z = 0$, b is the specific buoyancy of the lifting gas, $d\vec{S} = \mathbf{n} dS$, $\mathbf{n}$ is the outward unit normal, dS is surface area measure on the strained balloon surface, w_f is the film weight per unit area, w_t is the tendon weight per unit length, $\tau \in \mathbb{R}^3$ is a parametrization of a deformed tendon $\Gamma \in \mathcal{S}$, w_{top} is the weight of the apex fitting, z_{top} is the height of w_{top}, W_f^* is the relaxed film strain energy density, W_t^* is the relaxed

tendon strain energy density. Relaxation of the film strain energy density is a way of modeling wrinkling in the balloon film and has been used in the analysis of pumpkin shaped balloons in [8].

To determine a strained equilibrium balloon shape, we solve the following:

$$\text{Problem } \star: \quad \min_{\mathcal{S}\in\mathcal{C}} \mathcal{E}(\mathcal{S}).$$

For the purpose of the analytical studies in this paper, we assume the differential pressure is in the form $P(z) = -bz - P_0$ where P_0 is known. We follow the convention that $-P(z) > 0$ means that the internal pressure is greater than the external pressure. $\mathcal{C}$ denotes the class of feasible balloon shapes. Here, the continuum problem is cast as an optimization problem. This approach is particularly well-suited for the analysis of compliant structures. In previous work, such as [8] and [9], Problem $\star$ was solved using Matlab software (`fmincon`). However, even when using the large-scale option and sparse matrices to conserve computer memory, we were unable to use `fmincon` to analyze more than 10 gores with an appropriately sized mesh. For this reason, Problem $\star$ was implemented into *Surface Evolver*. In the past, *Surface Evolver* was used to model natural-shape zero-pressure balloons where wrinkling was represented by a virtual fold (see [10]).

3 Stability

The degrees of freedom (DOF) in a faceted balloon shape $\mathcal{S}$ are the coordinates of the facet nodes that are free to move. Let $\mathbf{x} = (x_1, x_2, \ldots, x_N)$ be a list of the DOF. Let $\mathcal{E}(\mathbf{x})$ be the total energy of a balloon configuration $\mathcal{S} = \mathcal{S}(\mathbf{x})$.

The gradient of $\mathcal{E}$ evaluated at $\mathbf{x}$ is the $N \times 1$ vector

$$\nabla\mathcal{E}(\mathbf{x}) = \left[\frac{\partial\mathcal{E}}{\partial x_i}(\mathbf{x})\right], i = 1,2,\ldots,N.$$

The Hessian of $\mathcal{E}$ evaluated at $\mathbf{x}$ is the $N \times N$ matrix,

$$H_{\mathcal{E}}(\mathbf{x}) = \left[\frac{\partial^2\mathcal{E}}{\partial x_i \partial x_j}(\mathbf{x})\right], \quad i = 1,2,\ldots,N, \quad j = 1,2,\ldots,N. \tag{8}$$

When a volume constraint is imposed, Eq. (8) must be modified. Depending on the mesh size and number of gores, N is between 85,000 and 350,000 in our studies. However, $H_{\mathcal{E}}$ is sparse. The lowest eigenvalue of $H_{\mathcal{E}}$ was calculated by inverse iteration. The matrix $H_{\mathcal{E}} - tI$ was sparse Cholesky factored, with the shift value t chosen to guarantee positive definiteness. The factored matrix was then used to iteratively solve $(H_{\mathcal{E}} - tI)\mathbf{x}_{n+1} = \mathbf{x}_n$, starting with a random vector $\mathbf{x}_0$, until the iteration converged, almost certainly producing the eigenvector of the lowest eigenvalue. See [13, Section 11.7, p. 493].

Table 1: Input parameters for pumpkin shape finding. In parametric studies n_g and r_B will be varied.

Description	Variable	Nominal Value
Number of gores	$p_1 = n_g$	290
Bulge radius (m)	$p_2 = r_B$	0.78
Constant pressure term (Pa)	$p_3 = P_0$	130
Buoyancy (N/m^3)	$p_4 = b$	0.087
Cap 1 length (m)	$p_5 = c_1$	50
Cap 2 length (m)	$p_6 = c_2$	55
Tendon weight density (N/m)	$p_7 = w_t$	0.094
Film weight density (N/m^2)	$p_8 = w_f$	0.344
Cap 1 weight density (N/m^2)	$p_9 = w_{c_1}$	0.1835
Cap 2 weight density (N/m^2)	$p_{10} = w_{c_2}$	0.1835
Payload (kN)	$p_{11} = L$	27.80
Top fitting weight (kN)	$p_{12} = w_{top}$	0.79

Definition 3.1 *Let $\mathcal{S} = \mathcal{S}(\mathbf{x})$ be an equilibrium configuration, i.e., a solution of Problem $\star$. We say $\mathcal{S}$ is* stable *if all the eigenvalues of $H_{\mathcal{E}}(\mathbf{x})$ are positive. We say $\mathcal{S}$ is* unstable *if at least one eigenvalue of $H_{\mathcal{E}}(\mathbf{x})$ is negative. We say that the stability of $\mathcal{S}$ is* indeterminate *if the lowest eigenvalue of $H_{\mathcal{E}}(\mathbf{x})$ is zero.*

4 Preliminaries

There are twelve parameters that go into the shape finding process for a pumpkin balloon: number of gores ($p_1 = n_g$), bulge radius ($p_2 = r_B$), constant pressure term ($p_3 = P_0$), buoyancy of lifting gas ($p_4 = b$), length of Cap 1 ($p_5 = c_1$), length of Cap 2 ($p_6 = c_2$), film weight density ($p_7 = w_f$), Cap 1 weight density ($p_8 = w_{c_1}$), Cap 2 weight density ($p_9 = w_{c_2}$), tendon weight density ($p_{10} = w_t$), suspended payload ($p_{11} = L$, includes weight of nadir fitting), and weight of apex fitting ($p_{12} = w_{top}$). See [1] for more on the pumpkin model. Typically, material properties such as film modulus and Poisson ratio do not enter directly into the shape finding process. We define the shape finding vector, to be

$$\begin{aligned}\mathbf{p} &= (p_1, p_2, \ldots, p_{12}) \\ &= (n_g, r_B, P_0, b, c_1, c_2, \ldots \\ &\qquad w_f, w_{c_1}, w_{c_2}, w_t, L, w_{top}).\end{aligned} \tag{9}$$

Table 2: Quantities related to the nominal pumpkin design, Phase IV-A: $(n_g, r_B) = (290, 0.78)$.

Description	Value
Volume (Mm^3)	0.590
Skin weight (kN)	13.33
Cap weight (kN)	3.51
Tendon weight (kN)	0.635
Tendon length (m)	155.30
Gore seam length (m)	155.93

The shape finding parameters that were used for the Phase IV-A design are presented in Table 1. Once a set of values are assigned to $\mathbf{p}$, the corresponding pumpkin design shape $\mathcal{S}_d(\mathbf{p})$ and lay-flat pattern $\Omega(\mathbf{p})$ are determined along with other quantities such as the total system weight, volume, tendon length and seam length of the lay-flat gore pattern (see Table 2). The three-dimensional shape $\mathcal{S}_d(\mathbf{p})$ is discretized (call it $\mathcal{S}_d(\mathbf{x};\mathbf{p})$), and $\mathcal{S}_d(\mathbf{x};\mathbf{p})$ is used as the initial guess for solving Problem $\star$ and determining the corresponding strained equilibrium shape $\mathcal{S}$. The tendon length is the edge length of $\mathcal{S}_d(\mathbf{p})$. By construction, the edge of the lay-flat pattern is longer than the tendon. To accommodate this lack-of-fit, the film along the seam is gathered before the tendon is attached. Note, local lack-of-fit varies along the length of the seam (i.e., more material must be gathered near the equator than near the poles).

Ideally, the unstrained tendon has no slackness and so each segment length in a tendon should match the corresponding length in $\mathcal{S}_d$. However, to properly model the tendon/film mismatch, we should allow for tendon slackness or additional tendon shortening and so we introduce the tendon uniform slackness parameter ε_t. In particular, if $\varepsilon_t = 0.005$, then a tendon segment must strain 0.5% before it comes under tension. If $\varepsilon_t = -0.005$, then each tendon segment length is shortened by an additional 0.5% beyond the local lack-of-fit due to the $\mathcal{S}_d(\mathbf{p})$ and $\Omega(\mathbf{p})$ mismatch. In theory, $\varepsilon_t = 0$, but to illustrate sensitivity to this parameter, we will let $\varepsilon_t = -0.008$ for the nominal case.

We are most interested in investigating the stability of equilibrium configurations of pumpkin designs as a function of (n_g, r_B), and for this reason, we define the following family of balloon designs,

$$\begin{aligned}\Pi_d \;=\; \{&\{\mathcal{S}_d(\mathbf{p}),\Omega(\mathbf{p})\}, p_1 \in \{48,49,\ldots,350\},\\ &\bar{r}_B(p_1) < p_2 < \infty,\ p_3, p_4, \ldots, p_{12}\\ &\text{as in Table 1}\},\end{aligned} \tag{10}$$

where $\bar{r}_B(n)$ is the smallest possible bulge radius for a design with n gores. For convenience, we will refer to a particular design in Π_d, by indicating the number of gores and the bulge radius. For example, $\{\mathcal{S}_d(290,0.78),\Omega(290,0.78)\}$ refers to the Phase IV-A design. If a parameter is not explicitly written out, it will be our convention that it is assigned a default value given in Table 1.

For each design in Π_d, it would also be of interest to know how stability depends on variations in the width of the lay-flat pattern. To study this dependency, we will consider two additional classes of designs $\Pi_d^{\pm}$ which we define in the following way. Let $\{\mathcal{S}_d(\mathbf{p}),\Omega(\mathbf{p})\} \in \Pi_d$. Let v denote arc-length as measured down the center of the lay-flat pattern. The gore half-width is a function of v and depends on the shape finding vector $\mathbf{p}$ (i.e., $h(v) = h(v;\mathbf{p})$). The lay-flat configuration in Π_d is given by

$$\Omega(\mathbf{p}) = \{(u,v) \mid 0 \le v \le \ell, -h(v) \le u \le h(v)\}. \tag{11}$$

We define

$$h_\delta^{\pm}(v) = \begin{cases} (1 \pm \delta)h(v), & v_1 < v < \ell - v_1 \\ h(v), & \text{otherwise.} \end{cases} \tag{12}$$

In our studies, $v_1 \approx 13$ m and $0 < |\delta| \le 0.015$; the gore is about 25 cm wide at v_1 and $\ell - v_1$. Eq. (12) generates new lay-flat patterns $\Omega^{\pm}(\mathbf{p})$, and we define

$$\Pi_d^{\pm} = \{\{\mathcal{S}_d(\mathbf{p}),\Omega^{\pm}(\mathbf{p})\},\ \{\mathcal{S}_d(\mathbf{p}),\Omega(\mathbf{p})\} \in \Pi_d\}. \tag{13}$$

Even though the lay-flat patterns are altered in $\Pi_d^{\pm}$, we utilize the three-dimensional shapes $\mathcal{S}_d(\mathbf{p})$ from Π_d, since they are used only to initiate the solution process in Problem $\star$. The nominal value of δ is assumed to be zero, unless otherwise specified.

Once, a design has been defined, then we can carry out a stress analysis of that design for some loading condition. Coming into play at this stage are other properties such as the film Youngs modulus ($q_1 = E_f$), film Poisson ratio ($q_2 = \nu$), Cap 1 Youngs modulus ($q_3 = E_{c_1}$), Cap 1 Poisson ratio ($q_4 = \nu_{c_1}$), Cap 2 Youngs modulus ($q_5 = E_{c_2}$), Cap 2 Poisson ratio ($q_6 = \nu_{c_2}$), tendon stiffness ($q_8 = E_t$), and the tendon slackness parameter ($q_7 = \varepsilon_t$). We define

$$\begin{aligned}\mathbf{q} &= (q_1, q_2, \ldots, q_8)\\ &= (E_f, \nu, E_{c_1}, \nu_{c_1}, E_{c_2}, \nu_{c_2}, E_t, \varepsilon_t),\end{aligned} \tag{14}$$

which includes parameters that were not used in the shape finding process. Nominal values for $\mathbf{q}$ are presented in Table 3. Once $\mathbf{p}$ and $\mathbf{q}$ are specified, we can proceed to solving Problem $\star$. Note, the shape determination process and the stress analysis process are separate processes, and so it is possible to use one value of a parameter in the shape finding process, and another value in the solution of Problem $\star$. The shape finding process defines the lay-flat gore

Table 3: Additional parameters for strained pumpkin shapes and default Phase IV-A parameters with $(n_g, r_B) = (290, 0.78)$.

Description	Variable	Value
Film Youngs modulus (MPa)	$q_1 = E_f$	404.2
Film Poisson ratio	$q_2 = \nu_f$	0.830
Cap 1 Youngs modulus (MPa)	$q_3 = E_{c_1}$	216
Cap 1 Poisson ratio	$q_4 = \nu_{c_1}$	0.830
Cap 2 Youngs modulus (MPa)	$q_5 = E_{c_2}$	216
Cap 2 Poisson ratio	$q_6 = \nu_{c_2}$	0.830
Tendon stiffness (MN)	$q_7 = E_t$	0.650
Tendon slackness (m/m)	$q_8 = \varepsilon_t$	-0.008

pattern $\Omega(\mathbf{p})$ and provides a three dimensional shape $\mathcal{S}_d(\mathbf{p})$ that is used for initializing the solution process for Problem $\star$. The strained equilibrium shape that is a solution of Problem $\star$ is denoted $\mathcal{S}(\mathbf{p}, \mathbf{q}, \Omega(\mathbf{p}))$. After solving Problem $\star$ with a design $\{\mathcal{S}_d, \Omega\} \in \Pi_d$, we will then classify the resulting strained equilibrium configuration according to Definition 3.1.

In our stability studies, we will consider nominal parameter values for $\mathbf{q}$ for each of the three classes, Π_d, Π_d^-, Π_d^+. We will also consider designs classes where we change some components of $\mathbf{p}$ or $\mathbf{q}$ from their nominal values. For example, we let $E_f \to \frac{1}{2}E_f$ and $P_0 \to \frac{1}{4}P_0$. We will also consider parameter studies where both ε_t and δ are varied.

Remark We note that stability of an equilibrium configuration is investigated at an equilibrium, which is a strained state. In general, a strained equilibrium shape is only approximately a cyclically symmetric constant bulge radius surface. Other strained equilibrium states (due to pressure variations or visco-elastic straining over time) depart from the cyclically symmetric constant bulge radius configuration even more. In the case of a visco-elastic film, that departure can be significant. As shown in this paper by way of looking at classes $\Pi_d^{\pm}$, this shape change can have profound effect on stability. While at this time we cannot look at complications that may arise from inflation path dependant locking of gores, our paper provides a step towards developing tools that lead to deployable, structurally efficient designs of pumpkin shape super-pressure balloons.

In a pumpkin balloon design that aims for structural efficiency, the maximum meridional stress resultant $\max \sigma_M$ anywhere along the gore length is at most as high as the maximum hoop stress resultant $\max \sigma_H$. Since the radius of curvature R_M for the meridional direction is much larger than r_B everywhere along the gore length, any relief in the hoop stress resultant due to a non-zero meridional stress resultant is insignificant, as demonstrated by the equilibrium equation

$$P = \sigma_H / r_B + \sigma_M / R_M. \tag{15}$$

In Eq. (15), P is the differential pressure, σ_H is the hoop stress resultant and σ_M is the meridional stress resultant. It follows that for the case of a constant bulge radius shape, the maximum hoop stress resultant is $\max \sigma_H \approx P_0 r_B$, where we use the fact that $bz_{top} << P_0$ and $P(z) = bz + P_0 \approx P_0$ (this is true for pumpkin ULDB's under consideration by NASA).

For strength efficiency, the designer would like to choose the smallest possible bulge radius. Its lower bound is roughly half the distance between adjacent tendons at the equator. There are practical limitations that discourage the designer from approaching this lower bound. Beyond those limitations there are also stability considerations, which are the subject of this paper.

For constant bulge radius designs with a fixed number of gores, the one with the smallest bulge radius is the one that has the most hoop-wise excess material relative to minimal gas bubble enclosure, which for the purpose of our discussion is the developable surface generated by straight lines (chords) that span adjacent tendons. This hoop-wise excess, if sufficiently large, can be detrimental to the stability of the cyclically symmetric configuration at float and under pressurization.

Still, for a small enough n_g, a minimum bulge radius design that approaches the lower bound is robustly stable as has been shown in the exploratory work [5] for 48 gore test vehicles and this is demonstrated analytically in this paper for even larger n_g. Calledine [11] showed that for constant bulge shape designs, increasing the number of gores also increases vulnerability to instability of the cyclically symmetric configuration. We demonstrate this fact analytically for nominally constant bulge radius designs.

Clearly, there is a need for design criteria that will enable the designer to arrive at structurally efficient designs while providing sufficient margins against the occurrence of instability with full consideration of the usual uncertainties, and in the case of a visco-elastic film also accounting for the service lifetime configuration changes of the balloon. Our exposition provides a description of how such design guidelines can be derived and demonstrates its feasibility.

5 Numerical studies

To begin our analysis of the Phase IV-A design, we calculated an equilibrium shape assuming the parameter values in Table 1. We denote this solution by $\mathcal{S}(290, 0.78)$. We find $H(\mathcal{S}(290, 0.78))$ has at least one negative eigenvalue and so we say that that $\mathcal{S}(290, 0.78)$ is unstable.

In the following, we consider a number of different numerical studies. Beginning with designs in Π_d, we determined the stability of the fully inflated/fully deployed strained equilibrium corresponding to each design. The nominal case is presented in Figure 3. To illustrate how the regions of stability and instability depend on various parameters in $\mathbf{p}$ or $\mathbf{q}$, we carried out a number of numerical studies where we altered one or two parameters, holding all the others at their nominal value.

In Figure 3, we present the parameter space for nominal designs. The lower bound $\bar{r}_B(n_g)$ was estimated numerically for each n_g. For each design $\{\Omega, \mathcal{S}_d\} \in \Pi_d$, we solved Problem $\star$ and determined the number of negative eigenvalues of $H(\mathcal{S})$. A square is plotted if the corresponding design leads to a stable equilibrium. A dot is plotted if the corresponding design leads to an unstable equilibrium. For clarity of exposition, we will consider Figure 3 as defining a baseline that consists of a stable and an unstable regions. Parameter sensitivity is detected by how the boundary between these regions changes for different parameter values.

Case I Consider designs in Π_d for nominal parameters. The stability results are summarized in Figure 3. We see that the Phase IV-A design has a bulge radius that is very close to $\bar{r}_B(290)$ and is right on the boundary separating stable shapes from unstable shapes.

Case II Consider designs in Class Π_d^-, where the nominal gore widths are narrowed using Eq. (12) and $\delta = -0.015$. The stability results are summarized in Figure 4. In (n_g, r_B) parameter space, we see that reducing the gore width, reduces the region of instability and increases the region of stability.

Case III Nominal design parameters and Π_d are used, except the constant pressure term is reduced from $P_0 = 130$ Pa to $P_0 = 32.5$ Pa. Stability results are presented in Figure 5. This study is relevant to a long duration flight that experiences many diurnal cycles. At night, the internal gas pressure will drop, and it will be important that the equilibrium configurations for these conditions remain stable.

Case IV Nominal parameters and Π_d are used, except film modulus E_f is decreased by 50%, i.e., $E_f = 202$ MPa. The results are presented in Figure 6 where we see that the region of instability has increased when the film modulus was decreased. This case study asserts the importance that the float equilibrium shape remain stable for all conditions, including those at end-of-service.

Case V Consider designs in Class Π_d^+, where the nominal gore widths are widened using Eq. (12) and $\delta = 0.015$. Stability results are presented in Figure 7. We see that adding "additional gore width" increases the region of instability in (n_g, r_B) parameter space.

Case VI Nominal design parameters and Π_d are used, except the slackness parameter is set to $\varepsilon_t = +0.005$. This means that the tendons have about 0.5% slackness. This plot suggests that a balloon with additional fore-shortening is more likely to be unstable than one without additional tendon fore-shortening. One must keep in mind that the local lack-of-fit is still enforced in both designs. If we assume that the fabricator has accounted for all the effects of tendon slackness but the local lack-of-fit is not done accurately, the chances for an unstable design are increased.

Case VII Nominal design parameters and Π_d^+ are used, but two parameters, ε_t and δ are changed, $(\varepsilon_t, \delta) = (-0.006, 0.01)$. See Figure 9.

Case VIII Nominal design parameters and Π_d^+ are used, but two parameters, ε_t and δ are changed, $(\varepsilon_t, \delta) = (0.0, 0.015)$. See Figure 10.

Our analytical notion of stability is consistent with the observational based notion of stability. However, the analytical definition of stability allows us to quantify the boundary between stable and unstable designs and provides guidelines to the balloon designer to avoid designs that can lead to unstable equilibria when fully inflated and full deployed. For example, if tolerances are known for the fabricated lay-flat gore pattern, stability curves similar to those presented in Figures 3-7 can be generated.

It is important to keep in mind, there are many other factors that the balloon designer must take into account. For example, to avoid over-stressing the film, designs with too few gores or designs with bulge radii too large may be rejected by the balloon designer, regardless of their stability. Most of the designs we consider are not practical. However, analyses of these cases allow exploration that aid our understanding of the causes of the instabilities that are of concern.

6 Experimental and flight data

Much of the available experimental data related to pumpkin balloons is presented in the format of chord ratio versus the number of gores. The maximum chord ratio is the maximum ratio of true gore width (rib length) to tendon-to-tendon width (chord length) (see [5, Figure 5]). For

Table 4: Stability Case Studies

Case	Design Class	Variation
I	Π_d	None
II	Π_d^-	$\delta = -1.5\%$
III	Π_d	$P_0 = 32.5$ Pa
IV	Π_d	$E_f = 202$ MPa
V	Π_d^+	$\delta = +1.5\%$
VI	Π_d	$\varepsilon_t = +0.5\%$
VII	Π_d^+	$(\delta, \varepsilon_t) = (1.\%, -0.6\%)$
VIII	Π_d^+	$(\delta, \varepsilon_t) = (1.5\%, 0.0\%)$

each rib, we calculate the ratio of the rib length (an arc of a circle of radius r_B) to the tendon-to-tendon (chord) length and then take the maximum of these ratios (denoted by max S/C). See Figure 1.

Calledine's work (see [11]) applied to the Endeavour balloon was the first analytical treatment that grappled with the deployment problem of a pumpkin-like balloon, and so, it has attracted much attention in the NASA ULDB circles. The Endeavour balloon was based on the dubious constant bulge angle pumpkin. However, constant bulge radius pumpkins were considered later by Lennon and Pellegrino (see [12]) using the Calledine definition of stability. Calledine's model is limited to hydrostatic pressure only, but his approach to stability is appropriate. Being limited by computational capabilities of the time, Calledine cleverly observed that in his semi-empirical approach he could ignore the variation in the strain energy contribution to the corresponding variation of the total potential energy. This allowed him to approximate the principle of the minimum total potential energy by a maximum volume rule. The computational simplification afforded by this approximate rule is significant. Calledine's approximation, even though formulated on the basis of a two-dimensional proxy-problem seems to be remarkably accurate. We include a comparison of our stability results with the Calledine results on a common grid in Figure 11. The curve in Figure 11 is reproduced from the paper by Schur and Jenkins (see [5, Figure 5], a figure reproduced from a plot provided by Mike Smith/Raven Industries). Note, Figure 11 plots the maximum chord ratio (max S/C) versus the number of gores. We computed max S/C for each design in Figure 3 and reproduced the stability results as a function of $(n_g, \max\ \text{S/C})$. We added additional members to Π_d, by calculating equilibria for $n_g = 48, 60$, and 75 and included these in Figure 11.

Remark Figure 11 includes a comparison of Calledine stability results and our stability results based on Definition 3.1 (indicated by BBS-stability in Figure 11). The reader should be reminded of two fundamental differences between the results. First, our stability criteria, Definition 3.1, includes strain energy, but the Calledine definition of stability does not. Second, our stability analyses are of constant bulge radius pumpkin designs, but the Calledine stability curve is based on analysis of constant bulge shape designs.

7 Conclusions

In this paper we analyzed a balloon design that is very similar to the Phase IV-A pumpkin balloon. Phase IV and Phase IV-A ULDB balloons with 290 gores experienced deployment problems. Our investigation identifies the Phase IV-A design as unstable. The nominal designs of the Phase IV-A balloons were identical but instructions given to the fabricator were different. This difference manifested itself in gore width shortfalls near both gore ends of the successfully deploying balloon. This observation appears to demonstrate the sensitivity of stability to bulge radius distribution. We note also that on the stability plot (Figure 11) where $\max S/C$ is plotted versus n_g, our design for Phase IV-A falls close to the border between stable and unstable equilibria. The same holds true for the stability plot of Figure 3 where r_B is plotted versus n_g. Both our observations and the observations made earlier in [5] are consistent with what has been observed on these flights.

The earlier Phase IV-A mission, Flight 1580PT in July 2002, was terminated by the failure of tendon anchorage on the nadir fitting owing to a fabrication error. We recognize that had that flight continued over a longer period, the equilibrium configuration could, as a result of creep, very well have migrated into an undesired configuration given the closeness of the design to the stability limit as identified by our investigation.

While much of the reporting on the stability of pumpkin shape balloons has been done in terms of the fabricated shape, stability is determined at the strained equilibrium configuration. Therefore it is appropriate to investigate design classes with a certain characteristic such as constant bulge radius in the deformed configuration and report stability limits in terms of geometric parameters of the equilibrium configuration. The design, i.e. the fabricated shape can be backed out using the appropriate elastic properties. For linear elastic materials this is straightforward. The design aid needed is a stability plot similar to Figure 3 for only one design scheme.

In the case of design schemes that use a film with visco-

elastic properties, the situation becomes more complicated as over time the equilibrium configuration changes due to visco-elastic strain and creep. Fortunately this change is systematic. For a constant bulge radius design at maximum pressure and at some elapsed time period under that pressure (that period should be chosen longer than the period for the transient response) the hoop-wise strain growth is slower at locations closer to the central axis of the balloon as the reduction of the length of the bulge radius due to strain is more rapid where the arc of the bulge is shallower. In addition to the design aid for the constant bulge radius design, similar plots for configurations that reflect the deformation history are required.

A design must of course stay well away from the stability limit for all possible service life configurations. The work presented in this paper does not provide the requisite design aids, but it demonstrates feasibility and method for the generation of such design aids.

Although the stability criteria of Definition 3.1 is a statement about a fully deployed/fully inflated equilibrium configuration, it also says something about the likelihood of a given design to deploy properly. For if the desired float shape is a cyclically symmetric unstable equilibrium configuration, and the real balloon corresponds, in all aspects including the pressurization state to the analytical model, then the balloon should not even be able to attain that cyclically symmetric float shape through a normal ascent. The successful deployments of the Phase II and Phase III balloons, and the failed deployments of the Phase IV and Phase IV-A balloons support our assertion.

Acknowledgment This research was supported in part by NASA Award NAG5-5353. The authors would like to thank George Washington University mathematics graduate student Michael Barg for assisting with the calculations needed for this paper.

References

[1] F. Baginski, "On the design and analysis of inflated membranes: natural and pumpkin shaped balloons," to appear in the SIAM Journal on Applied Mathematics.

[2] F. Baginski and W. Schur, "Design Issues for Large Scientific Balloons," AIAA-2003-6788, 3rd Annual Aviation Technology, Integration, and Operations (ATIO) Technical Forum, Denver, CO, October 2003.

[3] W. W. Schur, "Analysis of load tape constrained pneumatic envelopes", AIAA-99-1526, 40th AIAA/ASME/ASCE/AHS/ASC Structures, Structural Dynamics, and Materials Conference, St. Louis, MO, April 1999.

[4] F. Baginski and W. Schur, "Undesired equilibria of self-deploying pneumatic envelopes," AIAA-2004-1734, 45th AIAA/ASME/ASCE/AHS/ASC Structures, Structural Dynamics & Materials Conference, Palm Springs, CA, 19-22 April 2004.

[5] W. W. Schur , and C. H. Jenkins, "Deployment destiny, stable equilibria, and the implications for gossamer design", AIAA-2002-1205, 43nd AIAA/ASME/ASCE/AHS/ASC Structures, Structural Dynamics and Materials Conference and Exhibit, Denver, CO, April 2002.

[6] K. Brakke, *The Surface Evolver*, Experimental Mathematics **1**:2 (1992) 141-165.

[7] F. Baginski, "Clefting in pumpkin balloons," accepted for presentation at 34th COSPAR Scientific Assembly, Paris, 2004.

[8] F. Baginski and W. Schur, "Structural Analysis of Pneumatic Envelopes: A Variational Formulation and Optimization-Based Solution Process," inflated high altitude balloons," *AIAA J.*, Vol. 41, No. 2, February 2003, 304-311.

[9] F. Baginski and W. Collier, "Modeling the shapes of constrained partially inflated high altitude balloons," *AIAA J.*, Vol. 39, No. 9, September 2001, pp. 1662-1672. Errata: *AIAA J.*, Vol. 40, No. 9, September 2002, pp. 1253.

[10] F. Baginski and K. Brakke, "Modeling ascent configurations of strained high altitude balloons," AIAA Journal, **36** No. 10 (1998), 1901-1910.

[11] Calledine, C.R. "Stability of the Endeavour Balloon" in Buckling of Structures, I. Elishakoff et al., eds., Elsevier Science Publishers, (1988) 133-149.

[12] Lennon, A., and Pellegrino, S. (2000) "Stability of Lobed Inflatable Structures," AIAA-2000-1728, 41st AIAA/ASME/ASCE/AHS/ASC Structural Dynamics, and Materials Conference and Exhibit, Atlanta, GA, April 2000.

[13] W. Press et al, Numerical Recipes in C, 2nd ed., Cambridge University Press, 1992.

Figure 3: Case I. Regions of stability for Π_d. Phase IV-A baseline.

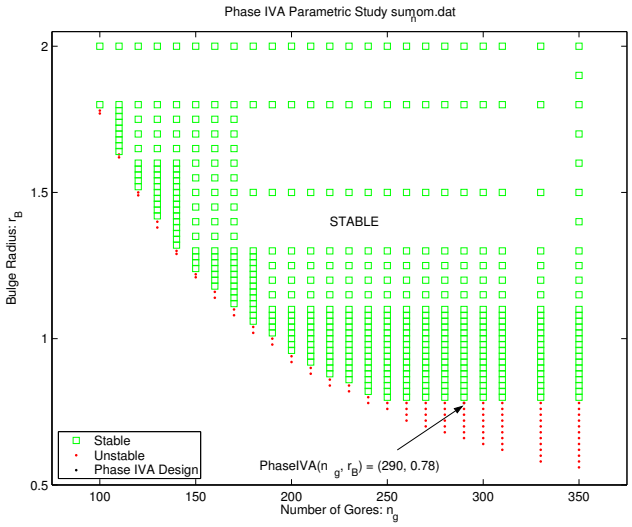

Figure 4: Case II. Regions of stability for Π_d^-. Lay-flat gores 1.5% narrower than nominal, $\delta = -1.5\%$.

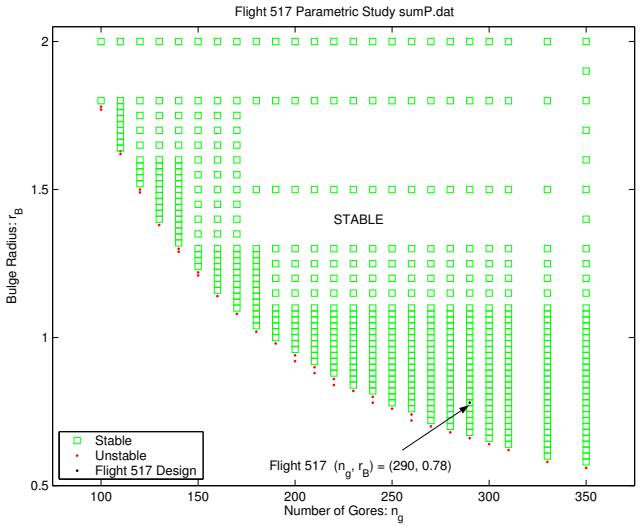

Figure 5: Case III. Regions of stability for Π_d-designs with reduced constant pressure term, $P_0 = 32.5$ MPa.

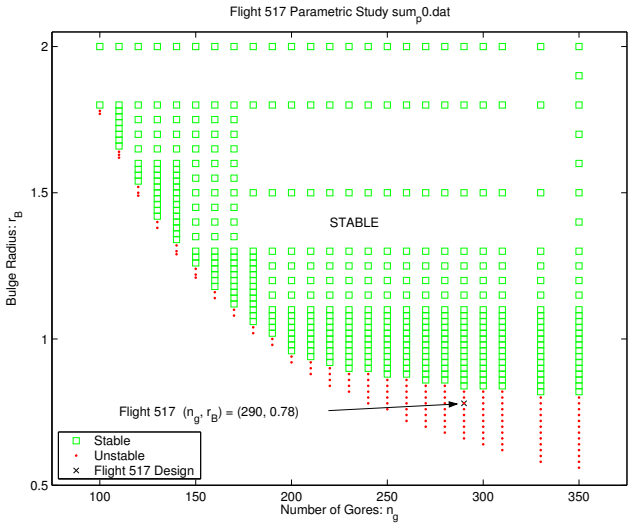

Figure 6: Case IV. Regions of stability for Π_d with film Youngs modulus reduced to $E = 202$ MPa.

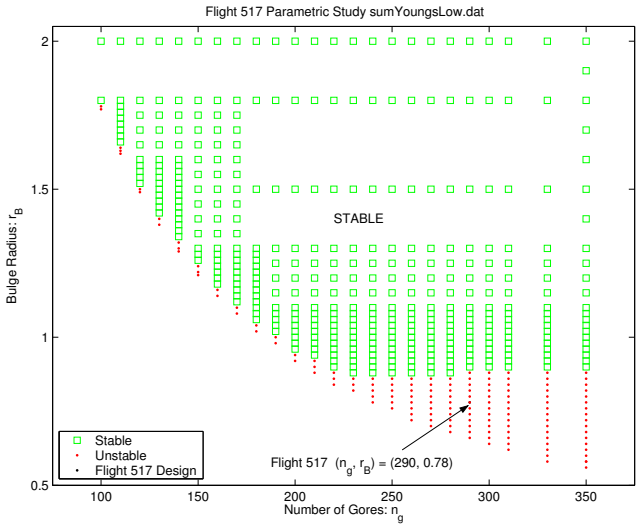

Figure 7: Case V. Regions of stability for Π_d^+. Lay-flat gores 1.5% wider than nominal. $(\delta, \varepsilon_t) = (0.015, -0.008)$.

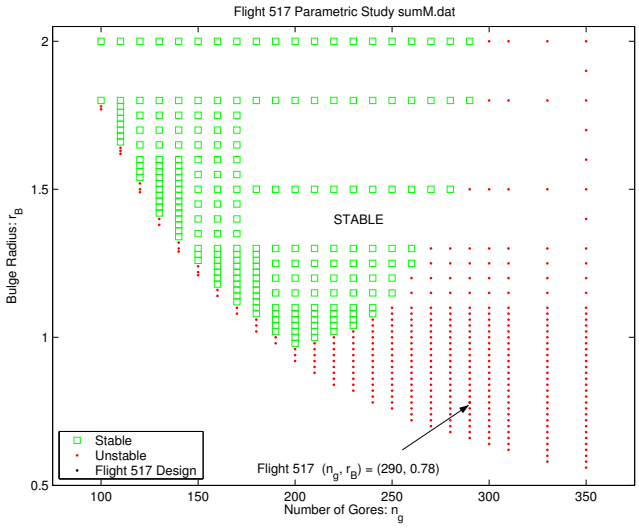

Figure 8: Case VI. Regions of stability for Π_d-designs, $(\delta, \varepsilon_t) = (0.0125, -0.007)$.

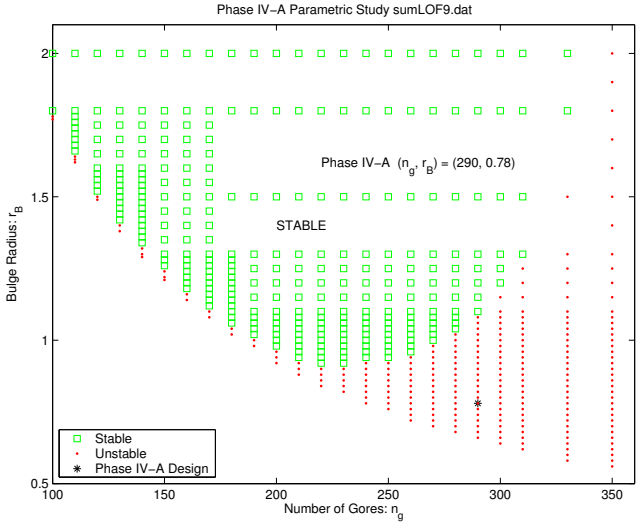

Figure 9: Case VII. Regions of stability for Π_d-designs, $(\delta, \varepsilon_t) = (0.01, -0.006)$.

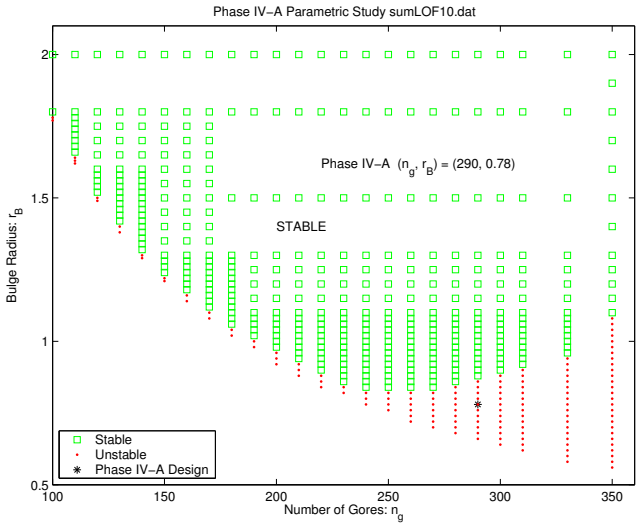

Figure 10: Case VIII. Regions of stability for Π_d-designs, $(\delta, \varepsilon_t) = (0.015, 0.0)$.

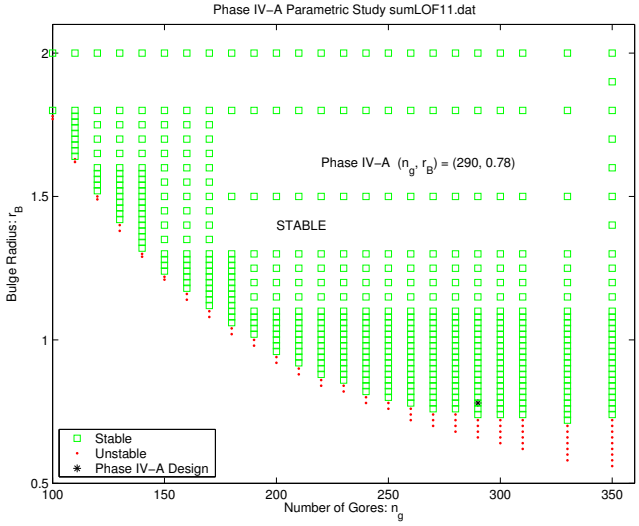

Figure 11: Regions of stability for variations on the Phase IV-A Design. Comparison of BBS-stability and Calledine stability. Calledine stability curve is maximum chord-width ratio (max S/C) versus number of gores as reproduced from [5, Figure 5]. Additional experimental and flight data are annotated in the figure.